Journal of Medicinal Chemistry

Article

Discovery of orally available runt-related transcription factor 3 (RUNX3) modulators for anticancer chemotherapy by epigenetic activation and protein stabilization

Jee Sun Yang, Chulho Lee, Misun Cho, Hyuntae Kim, Jae Hyun Kim, Seonghwi Choi, Soo Jin Oh, Jong Soon Kang, Jin-Hyun Jeong, Hyun-Jung Kim, and Gyoonhee Han

J. Med. Chem., **Just Accepted Manuscript** • DOI: 10.1021/acs.jmedchem.5b00062 • Publication Date (Web): 26 Mar 2015

Discovery of orally available runt-related transcription factor 3 (RUNX3) modulators for anticancer chemotherapy by epigenetic activation and protein stabilization

Jee Sun Yang[§], Chulho Lee[§], Misun Cho[§], Hyuntae Kim[‡], Jae Hyun Kim[‡], Seonghwi Choi[‡], Soo Jin Oh[†], Jong Soon Kang[†], Jin-Hyun Jeong[#,], Hyun-Jung Kim[fl], Gyoonhee Han[§,‡,*]*

[§] Translational Research Center for Protein Function Control, Department of Biotechnology, Yonsei University, Seodaemun-gu, Seoul 120-749, Republic of Korea

[†] Bioevaluation Center, Korea Research Institute of Bioscience and Biotechnology, Ochang, Cheongwon, Chungbuk 363-883, Republic of Korea

[#] College of Pharmacy and Yonsei Institute of Pharmaceutical Sciences, Yonsei University, Yeonsu-gu, Incheon 406-840, Republic of Korea

[fl] College of Pharmacy, Gachon University of Medicine and Science, Incheon 406-799, Republic of Korea

[‡] Department of Biomedical Sciences (WCU Program), Yonsei University, Seodaemun-gu, Seoul 120-749, Republic of Korea

KEYWORD: runt-related transcription factor 3 (RUNX3), histone deacetylase inhibitors, hydroxamic acids, pyridones, property, metabolic stability

ABSTRACT. Recently, we identified a novel strategy for anticancer chemotherapy by restoring runt-related transcription factor 3 (RUNX3) levels via lactam-based histone deacetylase (HDAC) inhibitors that stabilize RUNX3. Described here are the synthesis, biological evaluation, and pharmacokinetic evaluation of new synthetic small molecules based on pyridone-based HDAC inhibitors that specifically stabilize RUNX3 by acetylation and regulate its function. Many of the newly synthesized compounds showed favorable RUNX activities, HDAC inhibitory activities, and inhibitory activities on the growth of human cancer cell lines. Notably, one of these new derivatives, (E)-N-hydroxy-3-(2-oxo-1-(quinolin-2-ylmethyl)-1,2-dihydropyridin-3-yl)acrylamide (**4l**), significantly restored RUNX3 in a dose-dependent manner and showed high metabolic stability, a good pharmacokinetic profile with high oral bioavailability and long half-life, and strong antitumor activity. This study suggests that pyridone-based analogues modulate RUNX3 activity through epigenetic regulation as well as strong transcriptional and post-translational regulation of RUNX3, and could be potential clinical candidates as orally available RUNX3 modulators for the treatment of cancer.

INTRODUCTION

The dynamic and reversible process of epigenetic regulation can contribute to multiple human diseases such as cancer, inflammation, and metabolic diseases.[1-5] Histone deacetylase (HDAC) proteins function as epigenetic erasers that catalyze the removal of acetyl groups from lysine residues of target histones to regulate many cellular processes. In cancer cells, in particular, histone deacetylase (HDAC) isoenzymes and the corresponding hypoacetylation of histones are

typically seen at high levels.[6-8] Significant efforts have gone into developing HDAC inhibitors in the field of oncology. Various HDAC inhibitors have shown potent anticancer efficacy for solid and hematological cancers; most of these are hydroxamic acid derivatives, such as suberoylanilide hydroxamic acid (SAHA; Vorinostat, Zolinza®) and trichostatin A (TSA) (Figure 1).[9] However, most potent epigenetic drugs, which are mainly targeted at histone proteins, show substantial limitations, such as epigenetic non-specificity (pleiotropic effects) and drug resistance.[1, 10, 11] To overcome these problems of epigenetic therapy, many researchers have focused on modifying non-histone proteins – transcription factors, chaperones, structural proteins, and tumor suppressors – for the treatment of various cancers.[12-16]

In recent studies, runt-related transcription factor 3 (RUNX3), which is associated with the transforming growth factor (TGF)-β signaling pathway, was reported as a tumor suppressor in multiple solid tumors, particularly gastric cancer.[17-19] RUNX3 activity is induced by the transcriptional activation and post-translational stabilization of RUNX3, and these processes are in turn controlled by the opposing actions of histone deacetylase (HDAC) and histone acetyltransferase (HAT).[20] Hypermethylation of the CpG islands in the RUNX3 promoter region and methylation of histones H3K9 and H3K27 lead to the recruitment of HDACs, and deacetylation of histone H3 by HDACs induces repression of the transcriptional expression of RUNX3 genes.[17, 21] On the other hand, RUNX3 acetylation by p300 (HAT) results in RUNX3 stabilization via protection against ubiquitin-mediated degradation.[17, 22-24] Therefore, epigenetic regulation and post-translational modification by HDACs are highly related to the tumor suppressor activity of RUNX3. We have previously reported that the restoration and stabilization of RUNX3 levels by HDAC inhibition using lactam-based HDAC inhibitors have the potential become the new approach for anti-cancer chemotherapy.[25]

In this paper, we tried to identify an orally available RUNX3 modulator using a series of pyridone-based HDAC inhibitors which showed remarkable metabolic stability than lactam-based HDAC inhibitors.[26] Pyridone-based HDAC inhibitors were screened by a cell-based RUNX3 transcriptional activation assay system to investigate the relationship between HDAC inhibitory activity and RUNX3 activity. Cell-based mechanistic studies, including metabolic stability measurements, as well as an *in vivo* xenograft assay, were performed using the screened compounds to identify candidates. Our results demonstrate that our pyridone-based derivatives contribute to RUNX3 stabilization through epigenetic regulation and strong post-translational acetylation of RUNX3. Furthermore, the selected compounds caused attenuation of lung cancer pathogenesis. The high potency, stability, pharmacokinetic profiles, and *in vivo* efficacy of these compounds indicate the possibility of orally available RUNX3 modulators for treating cancer.

RESULTS AND DISCUSSION

Chemistry. The general procedure for the synthesis of pyridone-based RUNX3 modulators is outlined in Scheme 1. Commercially available pyridone carbaldehyde and Wittig reagent were refluxed in dichloromethane by the Wittig reaction to give *(E)*-methyl 3-(2-oxo-1,2-dihydropyridin-3-yl)acrylate (**1**). Compound **3** was produced from an *N*-alkylation reaction between commercial or synthetic aromatic alkyl halide **2** and compound **1**. The hydroxamic acid-based RUNX3 modulator series represented by **4** was obtained by reacting the esters of the pyridone with $KONH_2$ (1.7 M in MeOH) in MeOH at low temperature.

Thirty-one pyridone-based analogues were newly designed and synthesized as RUNX3 modulators based on our previously synthesized HDAC inhibitors[25-27]. The pyridone core and a conjugated system with an olefin connecting the hydroxamic acid moiety were retained for

metabolic stability against hydrolysis. For structure-activity relationship studies, the carbon chain linker between the cap group and the pyridone core was varied in length from one to three. Furthermore, diverse functional groups, such as bromophenyl, ethylphenyl, methoxyphenyl, or a solubilizing group (amine-containing heterocyclic group, such as pyridinyl or quinolinyl) were introduced as the cap group in these HDAC inhibitors to improve their RUNX activity and pharmacokinetic profiles.

Biological evaluation. RUNX transcriptional activity in the presence of synthesized pyridone-based analogues was evaluated using the luciferase assay system in 6xOSE2-C2C12 stable cells which are very efficient and useful system for screening of the transcriptional activity of RUNX2.[25, 28] Fibroblast growth factor 2 (FGF-2), which stimulates RUNX2 expression and function, was used as a positive control. RUNX activities are tabulated as percentage of activation compared to that seen with FGF-2. Inhibition of HDAC activity and cancer cell growth by pyridone-based analogues were monitored by the HDAC Fluorescent Activity Assay kit and the sulforhodamine B (SRB) assay, respectively. Six human cancer cell lines, PC-3 (prostate), MDA-MB-231 (breast), ACHN (renal), HCT-15 (colon), NCI-H23 (non-small cell lung), and NUGC-3 (gastric), were used in the SRB assay. The results are tabulated as 50% inhibitory concentration (IC_{50}) or 50% growth inhibition (GI_{50}) values in the micromolar range (Table 1). For these activity tests, SAHA was used as a reference for the comparison of *in vitro* activities.

As shown in Table 1, most of the evaluated compounds, with the exception of compounds containing a pyridinyl moiety on the cap group (**4i**, **4j**, **4k**, **4u**, **4v**, and **4e'**), showed favorable RUNX activities, HDAC inhibitory activities, and growth inhibitory activities against human cancer cells. Among these compounds, 9 of the pyridone-based analogues (**4g**, **4l**, **4o**, **4p**, **4t**, **4w**,

4x, **4b'**, and **4d'**) induced RUNX activation by over 100% while SAHA showed moderate RUNX activity at 80.2%. Moreover, three analogues, **4g**, **4l**, and **4w**, induced RUNX activity to greater than 150% (200.0%, 687.5%, and 162.8%, respectively). All of these RUNX-activating analogues also showed potent HDAC inhibition with an average IC_{50} value of 0.12 μM. In particular, compound **4l** activated RUNX and inhibited the HDAC enzyme as well as the growth of six cancer cell types even more thoroughly than did SAHA.

Structure-activity relationship (SAR) study of pyridone-based analogues. Initially, in order to assess the effects of the length of carbon chain between the pyridone core and the cap group, the compounds were divided into three groups based on the length of the spacer: the one-carbon linker group (**4a-4h** and **4l**), two-carbon linker group (**4m-4t**), and three-carbon linker group (**4w-4d'**) (Table 1). The activity data of pyridinyl-substituted compounds were not grouped with those of other compounds because of their extraordinarily poor activities on RUNX and on cancer cell growth inhibition. In terms of RUNX activity, compounds with one-carbon linkers were almost two-fold more active than compounds with two- or three-carbon linkers. On the other hand, the HDAC inhibition and cell growth inhibition activities of these compounds were almost the same regardless of their carbon chain length. If we fix the substituents of compounds to 3-methoxyphenyl, it is certain that compound with one-carbon linker (**4g**) possesses more potent RUNX activity than other compounds with higher-carbon linkers (**4q** and **4b'**). Also, their HDAC inhibitory activities are varied from 0.03 to 0.15 μM (4g = 0.15, 4q = 0.07, and 4b' = 0.03 μM). Especially, compound **4g** exhibited the lowest HDAC inhibitory activity while it induced RUNX activation by 200%. These results show that HDAC inhibitory activity of the synthesized compounds are not correlated to the RUNX activities although our compounds were designed on the model of HDAC inhibitors,

To evaluate the effects of different substituents at the cap group of the title compounds, diverse substituents, such as bromophenyl, ethylphenyl, pyridinyl, quinolinyl, *t*-butyl phenyl, ethoxyphenyl and methoxyphenyl, were introduced. On the whole, compounds with methoxy or quinolinyl substituents at the cap group showed favorable RUNX activity and HDAC inhibitory activities. In contrast, compounds with pyridinyl groups showed poor RUNX activities (<70 %) and HDAC inhibitory activities as mentioned above. Also, to assess the effects of the position of the substituents, bromophenyl substituted compounds (**4a** – **4c**) were prepared. The carbon chain length of the selected compounds was fixed to one carbon, which was previously stated to have superior RUNX activity than the compounds with two- or three-carbon linkers. They activated RUNX similarly (around 90 %) regardless of the position of the substituents (ortho-, meta-, or para-position) and exhibited HDAC inhibitory activities with IC_{50} value of 0.19, 0.38, and 0.10 μM, respectively. These results show that the position of the substituents does not seriously affect the RUNX activities and it was affirmed again that the RUNX activation has no correlation with the HDAC inhibitory activity. .

Among the synthesized compounds, **4l** (n=1, R=2-quinolinyl), **4o** (n=2, R=4-ethyl), **4p** (n=2, R=4-t-butyl), **4b'** (n=3, R=3-methoxyphenyl) and **4d'**(n=3, R=2-ethoxy) showed comparatively high inhibition not only of RUNX activity but also of human cancer cell growth. Compound **4l** exhibited the most potent cancer cell growth inhibitory activities (GI_{50} = 0.10–0.71 μM) and HDAC inhibitory activity (IC_{50} = 30 nM) as well as RUNX activity (relative RUNX transcriptional activation to FGF-2 = 687.5%).

Regulation of RUNX3 acetylation. RUNX3 acetylation is reported to be essential for the maintenance of RUNX3 stability.[22] To assess RUNX3 stability, we evaluated RUNX3 acetylation and protein levels after treating cells with our synthesized compounds. Nine

compounds with over 100% RUNX activity were selected for evaluation from among 31 synthesized compounds. The well-characterized anti-cancer drug TSA, a HDAC inhibitor, was used as a positive control.

Among the tested compounds, **4g**, **4l**, **4w,** and **4d'** significantly increased the levels of acetylated RUNX3 compared to the positive control (Figure 2). These compounds also achieved strong stabilization of the RUNX3 protein. The RUNX3 acetylation levels of these compounds were even higher than that of SAHA, which showed a 14.1-fold greater RUNX3 acetylation level over that of the reference compound, TSA. In particular, compound **4l** dramatically increased the acetylation of RUNX3 to 77.5-fold higher than that seen with TSA (Figure 2B). However, the HDAC inhibitory activities of these four compounds displayed a wide spectrum (from 0.03 μM to 0.48 μM), indicating that HDAC inhibitory activities and RUNX3 acetylation do not have a quantitative relationship.

RUNX3 mRNA expression. According to the previous experiments, compound **4l** was chosen for further evaluation of RUNX3 mRNA expression and RUNX3 stability to determine whether it regulates RUNX3 at the transcriptional level. The expression of RUNX3 mRNA was determined in a lung cancer cell line, NCI-H460, by RT-PCR. In this cell line, due to hypermethylation of the CpG island in the promoter region, RUNX3 is not expressed in the normal condition. However, when treated with an HDAC inhibitor RUNX3 expression is restored.[21] SNU16 gastric cancer cells, which do not have a deletion in the RUNX3 locus and normally express RUNX3, were used as a positive control.

As shown in Figure 3, Compound **4l** induced RUNX3 mRNA expression in a dose-dependent manner. The increased levels of RUNX3 mRNA induced by 0.1 and 1 μM **4l** were comparable to

that induced by SAHA. Furthermore, 10 μM **4l** showed strong effects on RUNX3 mRNA expression in comparison with SAHA. This result shows that compound **4l** successfully reactivated the tumor suppressor gene RUNX3.

Metabolic stability in mouse, rat, and human liver microsomes. In parallel with the RUNX3 acetylation experiments, metabolic stability profiles were evaluated in mouse liver microsomes for the nine selected compounds that exhibited the greatest RUNX transcriptional activation over 100%. In addition, we calculated the values of lipophilicity (AlogP) and polar surface area (PSA) of the selected compounds using Discovery Studio 4.0™ (Table S2).

We previously confirmed that the enzymatic hydrolysis properties of these compounds can be improved by replacing the gamma- or delta-lactam core with a pyridone core.[26] The double bond conjugation system of hydroxamic acid with the pyridone structure improved metabolic stability against hydrolysis of the carboxyl acid. As a consequence, the newly synthesized pyridone-based analogues (**4g**, **4l**, **4o**, **4p**, **4t**, **4w**, **4x**, **4b'**, and **4d'**) were resistant to hydrolysis (Table 2). In the presence of NADPH in mouse liver microsomes, which are involved in the NADPH-dependent cytochrome P450 (CYP450)-mediated oxidative reaction, **4g**, **4l**, **4t** and **4b'** (61.5%, 90.3%, 59.6%, and 88.4% remaining, respectively) were more stable than other compounds. Furthermore, the compounds that showed metabolic instability had higher lipophilicity (AlogP values >2.0) than comparably stable compounds. The instability of these compounds can be explained based on the previous observation that metabolic instability results from the high lipophilicity of compounds in mouse liver microsomes[29].

In vitro phase I and II metabolic stability in rat liver microsomes was assessed for compounds **4l** and **4b',** which showed the greatest stability in mouse liver microsomes, and the data are

summarized in Table 3. In phase I metabolism, both compounds exhibited good stability against metabolic hydrolysis and oxidative reactions, as seen in mouse liver microsomes. However, uridine 5'-diphospho-glucuronic acid (UDPGA)-dependent phase II metabolism was observed for compound **4b'** (45.7% remaining). Based on several studies of the metabolism of hydroxamic acid derivatives[30-32], the hydroxamic acid moiety of **4b'** seems to be metabolized by *O*-glucuronidation. Compound **4l**, however, was stable against UDPGA-dependent metabolism in rat liver microsomes, with 72.4% remaining. Similar stability results with respect to the phase I and phase II metabolism of **4l,** and even better values with respect to glucuronidation, were seen in human liver microsomes. Among these, **4l**, which contains a quinolinyl moiety, emerged as the most stable compound against NADPH- and UDPGA-dependent metabolism. As a result, introducing a quinolinyl moiety at the cap group in pyridone-based analogues improved microsomal stability.

Pharmacokinetic profiles. Compound **4l**, which caused high RUNX3 acetylation level and high stability against enzymatic hydrolysis and oxidation, was selected for *in vivo* pharmacokinetic evaluation. The pharmacokinetics of **4l** administered intravenously and orally at 2 mg/kg and 10 mg/kg, respectively, was evaluated in male Sprague-Dawley (SD) rats. The systemic exposure, clearance, and steady state volume of distribution of **4l** were 354.5 ng·hr/ml, 5.6 l/hr/kg, and 4.4 l/kg, respectively (Table 4). After oral administration, **4l** exhibited high exposure, as 863.3 ng·hr/ml. This high oral exposure level seems to be correlated with the stability in liver microsomes. The terminal half-lives of **4l** were approximately 4.4 and 10.3 h after intravenous and oral dosing, respectively. Moreover, the oral bioavailability for **4l** was found to be 48.7% at 10 mg/kg oral dose. Compound **4l** showed significant improvement in $t_{1/2}$ and oral bioavailability, and these values were competitive with those of SAHA.[33]

Reduced tumor growth in xenograft models. We evaluated the most active and stable compound **4l** in *in vivo* xenograft experiments to assess antitumor activity and toxicity (body weight loss). NCI-H460 cells were subcutaneously implanted into nude mice. Compound **11-8**, for which we have previously reported antitumor activity in gastric cancer cells following intravenous injection, was used as a positive control.[25] Compounds **4l** and **11-8** were administered orally at 20 mg/kg daily for 2 weeks. Tumor volumes were measured every 2 or 3 days for 14 days.

As shown in Figures 4A and 4B, treatment with **4l** caused a dramatic reduction in tumor growth without significant body weight loss. Notably, **4l** showed increased antitumor activity compared to **11-8** (45.71% and 38.08%, respectively), indicating that its improved metabolic stability and activity may contribute to increased clinical availability. As shown in Figure 4C, **4l** significantly decreased the tumor weight by 45.70%, while **11-8** resulted in a 37.93% reduction. These results imply that this new class of RUNX3 modulators could be applied in new cancer therapeutics. In pharmacokinetic-pharmacodynamic (PK–PD) studies, two-fold higher levels of **4l** were also observed in tumors as compared to **11-8** (Supplementary Figure S1), which correlates with the anti-tumor effect observed in the xenograft model.

CONCLUSION

Thirty-one pyridone-based analogues were designed and synthesized as RUNX3 modulators to improve potency and pharmacokinetic profiles. Most of the pyridone-based compounds excluding those with pyridinyl substituents at the cap group exhibited favorable RUNX activity and cancer cell growth inhibitory activities. RUNX3 stability and metabolic stability were evaluated for nine compounds which exhibited outstanding RUNX activities. Among them, **4l**

resulted in remarkably increased RUNX3 acetylation level and RUNX3 mRNA expression, showing that it can successfully stabilize RUNX3 through epigenetic regulation and strong post-translation regulation of RUNX3. Furthermore, **4l** emerged as the most stable compound against NADPH- and UDPGA-dependent metabolism. Introducing a quinolinyl moiety is expected to result in metabolic blocking of CYP-mediated oxidation and glucuronidation. The superior metabolic stability of **4l** resulted in a good pharmacokinetic profile with high oral bioavailability and long half-life and understandably reduced tumor growth. Taken together, the data presented here suggest that compound **4l** represents a promising clinical candidate as an orally available RUNX3 modulator for the treatment of cancer.

EXPERIMENTAL SECTION

Chemistry. All chemicals were obtained from commercial suppliers and used without further purification. All reactions were monitored by thin-layer chromatography (TLC) on pre-coated silica gel 60 F_{254} (mesh) (Merck, Mumbai, India), and spots were visualized under UV light (254 nm). Flash column chromatography was performed with silica (Merck EM9385, 230-400 mesh). ^{1}H and ^{13}C nuclear magnetic resonance (NMR, Varian Unity Inova) spectra were recorded at 400 and 100 MHz, or at 500 and 125 MHz. Proton and carbon chemical shifts are expressed in ppm relative to internal tetramethylsilane, and coupling constants (*J*) are expressed in Hertz. Splitting patterns were presented as s, singlet; d, doublet; t, triplet; q, quartet; dd, double of doublets; m, multiplet; br, broad. Liquid chromatography-mass spectrometry (LC-MS) spectra were recorded by electrospray ionization (ESI) probe using a Shimadzu LC–MS2010 instrument with an Agilent C_{18} column, 50×4.6 mm, 5 μm particle size; mobile phase: 0.1% formic acid in H_2O/0.1% formic acid in CH_3CN (1:9) over 10 min; flow rate: 0.2 ml min^{-1}; scan mode (0–500 $amuz^{-1}$). The detected ion peaks were $(M^{+}z)/z$ in positive where M represents the molecular weight of the

compound and z represents the charge (number of protons). High-resolution ESI-MS measurements were performed on a Micromass Quadrupole-Time of Flight (Q-TOF) Acquity UPLC-Mass System at Yonsei University; positive mode. To determine the purity of the final compounds (**4a**−**4e'**), high performance liquid chromatography (HPLC) experiments were conducted using the Agilent analytical column Eclipse-XDB-C_{18} (150×4.6 mm, 5 μm) on Shimadzu HPLC 2010 instruments. All compounds tested in biological assays were ≥95% pure. Conditions and retention times are described in Supporting Information (Table S1). Cell lines were obtained from R&D Systems (Minneapolis, MN, USA).

General procedure for the preparation of title compounds 4a-4e'. To a solution of acrylate **3a-3f'** in anhydrous methanol (10.0 ml/mmol), under N_2 atmosphere, 1.7 M $KONH_2$ (5.0 equiv) was added at 0°C. The mixture was stirred for 12 h. The mixture was concentrated *in vacuo* and the crude product was purified by column chromatography (silica gel, 5 % methanol in dichloromethane) to afford the final pure product.

***(E)*-N-hydroxy-3-(2-oxo-1-(quinolin-2-ylmethyl)-1,2-dihydropyridin-3-yl)acrylamide (4l).** Yellow solid (26 mg, 22%). ^{1}H NMR (500 MHz, DMSO-*d6*) δ 8.34 (d, 1H, J =8.0 Hz), 7.97-7.94 (m, 2H), 7.88 (d, 1H, J =7.5 Hz), 7.78-7.71 (m, 2H), 7.57 (t, 1H, J =5.0 Hz), 7.41 (d, 1H, J =9.0 Hz), 7.33 (d, 1H, J =15.0 Hz), 7.06 (d, 1H, J =15.5 Hz), 6.43 (t, 1H, J =7.0 Hz), 5.44 (s, 2H); ESI (m/z) 322 (MH^+), 344 (MNa^+); HRMS (ESI) calculated for $C_{18}H_{15}N_3O_3$ [MH^+] 322.1191, found 322.1185; HPLC (^{t}R : purity = 9.606 min, 99.7 %).

***(E)*-N-hydroxy-3-(1-(3-(3-methoxyphenyl)propyl)-2-oxo-1,2-dihydropyridin-3-yl)acrylamide (4b').** Ivory solid (171 mg, 45%). ^{1}H NMR (400 MHz, DMSO-*d6*) δ 10.71 (s, 1H), 8.91 (s, 1H), 7.73 (d, 1H, J = 8.0 Hz), 7.66 (d, 1H, J = 6.8 Hz), 7.31 (d, 1H, J = 15.6 Hz),

7.15 (t, 1H, *J* = 8.0 Hz), 7.08 (d, 1H, *J* = 15.2 Hz), 6.755-6.705 (m, 3H), 6.29 (t, 1H, *J* = 6.8 Hz), 3.94 (t, 2H, *J* = 7.2 Hz), 3.69 (s, 3H), 2.55 (t, 2H, 7.8 Hz), 1.966-1.891 (m, 2H); ESI (m/z) 329 (MH^+), 351 (MNa^+); HRMS (ESI) calculated for $C_{18}H_{20}N_2O_4$ [MH^+] 329.1501, found 329.1493; HPLC (^tR : purity = 11.335 min, 99.0 %).

***(E)*-3-(1-(3-(2-ethoxyphenyl)propyl)-2-oxo-1,2-dihydropyridin-3-yl)-N-hydroxyacrylamide (4d').** Brown solid (145 mg, 44%). ^1H NMR (400 MHz, DMSO-*d6*) δ 10,71 (s, 1H), 8.88 (s, 1H), 7.74 (d, 1H, *J* = 6.4 Hz), 7.66 (d, 1H, *J* = 7.2 Hz), 7.31 (d, 1H, *J* = 15.6Hz), 7.11-7.07 (m, 3H), 6.87 (d, 1H, *J* = 8.4 Hz), 6.81 (t, 1H, *J* = 7.4 Hz), 6.29 (t, 1H, *J* = 6.6 Hz), 3.97-3.91 (m, 4H), 2.52 (t, 2H, *J* = 7.4 Hz), 1.88 (t, 2H, *J* = 7.4 Hz), 1.23 (t, 3H, *J* = 7.0 Hz); ESI (m/z) 343 (MH^+), 365 (MNa^+); HRMS (ESI) calculated for $C_{19}H_{22}N_2O_4$ [MH^+] 343.1658, found 343.1649; HPLC (^tR : purity = 12.367 min, 98.4 %).

Cell Cultures. All tissue culture media and antibiotics were purchased from Hyclone (Logan, UT, USA). HEK293 and C2C12-6xOSE cells were maintained in Dulbecco's modified Eagle medium (DMEM) with 10% fetal bovine serum (FBS) and antibiotics [penicillin (100 IU/ml), streptomycin (100 mg/ml)] (Invitrogen, Grand Island, NY, USA) at 37°C in a 5% CO_2 atmosphere. NCI-H460 and SNU16 cells were maintained in RPMI1640 media with 10% FBS and antibiotics. Treatment with 2 mM isopropyl-β-D-thiogalactopyranoside (IPTG, Sigma-Aldrich, St. Louis, MO, USA) was performed for 24 h to induce RUNX3 expression. Drugs were then added to cell cultures for an additional 24 h to assess effects on RUNX3 stability.

Screening for RUNX activity. The percentage of RUNX transcriptional activation relative to FGF-2 was determined using the C2C12-6xOSE cell line with the luciferase assay system. The C2C12-6xOSE cell line was kindly provided by Prof. Hyun-Mo Ryoo (Seoul National

University, Seoul, South Korea). Cells were plated at 1×10^4 cells per well in 96-well plates. Fibroblast growth factor (FGF)-2 and drugs (1 μM each) were added to cells the next day. After 24 h, cells were harvested and analyzed by luciferase assay with the Bright-Glo Luciferase Assay System according to the manufacturer's protocol (Promega, Madison, WI, USA). Lysates were analyzed with the GloMax-multi Detection System (Promega). FGF-2 was used as a positive control for RUNX activation.

HDAC inhibitory assays. The IC_{50} values of HDAC inhibitors were determined using the HDAC fluorometric assay/drug discovery kit (BioMol, now ENZO Life Science, Plymouth Meeting, PA, USA) which is based on the unique *Fluor de Lys*® system (Fluorogenic histone deacetylase lysyl substrate/developer). It is designed to measure histone deacetylases (HDAC) activity. In this assay, we used nuclear extracts from the human cervical cancer cell line HeLa (from 6 to 9 mg protein/ml in 0.1 M KCl, 20 mM HEPES/NaOH, pH 7.9, 20 % (v/v) glycerol, 0.2 mM EDTA, 0.5 mM DTT, 0.5 mM PMSF).[34] The HeLa cell nuclear extract contained all class I HDACs (HDAC1, HDAC2, HDAC3 and HDAC8), class II HDACs (HDAC4–7, 9 and 10), and human homolog of yeast Sir2 , SIRT1. SAHA was used as the positive control. A nuclear fraction of HeLa cells (15 μl of 30×) was diluted to 10 μl with the assay buffer containing the HDAC inhibitors and the *Fluor de lys*® substrate (lysine with an acetylated amino group on the side chain) at a final concentration of 100 μM. The samples were incubated for 30 min at 37°C and then added to the *Fluor de lys*® developer (25 μl) for 10 min at RT). The samples were measured using microtiter-plate-reading fluorimeter capable of excitation at a wavelength at 360 nm and detection of emitted light at 460 nm.

Cancer cell growth inhibitory assays. The final concentrations of reagent used to treat cells were 0.1, 0.3, 1, 3, and 10 μg/ml. Cells were harvested from exponential phase cultures by trypsinization, counted, and plated into 96-well plates. Optimal seeding densities for various human tumor cell lines (HCT-15, PC-3, NUGC-3, ACHN, MDA-MB-231, and NCI-H23) were determined to ensure exponential growth during a 5-day assay. The sulforhodamine B assay was performed with minor modifications.[35] The culture medium was aspirated prior to fixation of the cells by the addition of 50 μl 50% cold trichloroacetic acid. After 1 h incubation at 4°C, cells were washed five times with deionized water. After 24 h, the cells were stained with 100 μl 1× Sulforhodamine B (SRB, Sigma-Aldrich, St. Louis, MO, USA) dissolved in 1% acetic acid for at least 30 min and subsequently washed four times with 1% acetic acid to remove unbound stain. The plates were left to dry at room temperature for 24 h; subsequently, bound protein stain was solubilized with 100 μl of 10 mM unbuffered Tris and the optical density (OD) was read at 540 nm.

Liver microsomal stability assay. Microsomal incubations were conducted in triplicate in 0.1 M potassium phosphate buffer (pH 7.4) in 8-well tube strips placed in a 8×12 rack (1.2 ml; VWR, Emeryville, CA). To study NADPH-dependent oxidative metabolism, the test compound (1 μM) was incubated with pooled mouse, rat, or human liver microsomes (final concentration: 0.5 mg/ml) in the presence of NADPH (final concentration: 1 mM) in a final volume of 160 μl. The reaction was started by adding 1 mM β-NADPH and was terminated at 0 and 30 min by the addition of 160 μl ice-cold acetonitrile containing an internal standard (IS). Buspirone was used as a positive control. The incubation mixtures were centrifuged at 910×g for 10 min. The supernatant was analyzed by liquid chromatography electrospray ionization tandem mass spectrometry (LC-ESI/MS/MS). The percent compound remaining was calculated from the peak

area ratios of the analyte to the IS. These experiments were performed at the KRIBB Bio-Evaluation Center (Chungbuk, Korea).

In silico physiological profiles. The AlogP, number of single rotatable bonds, and fast PSA were calculated by Discovery Studio 4.0 (Accelrys, San Diego, CA).

Western blot analysis. After cells were lysed with radio-immunoprecipitation assay (RIPA) buffer (25 mM Tris-HCl, pH 7.6, 150 mM NaCl, 1% NP-40, 1% sodium deoxycholate, 0.1% sodium dodecyl sulfate, SDS), protein concentrations were determined with a bicinchoninic iacid assay (BCA) protein assay kit (Pierce, Rockford, IL, USA). Equal amounts of protein were fractionated by SDS-polyacrylamide gel electrophoresis (PAGE) and transferred onto a nitrocellulose membrane (BioRad, Richmond, CA, USA). After blocking with 5% skim milk in phosphate-buffered saline (PBS) containing 0.1% Tween 20, membranes were incubated with the appropriate primary antibodies at 4°C overnight. Proteins were detected with horseradish peroxidase (HRP)-conjugated secondary antibodies and an enhanced chemiluminescence (ECL) kit (Amersham Pharmacia Biotech, Buckinghamshire, UK). Antibodies against myc (9E10) and tubulin were from Santa Cruz Biotechnology (Santa Cruz, CA, USA). Anti-acetylated lysine antibody was purchased from Cell Signaling (Danvers, MA, USA).

Immunoprecipitation analysis. The myc-RUNX3 expression vector was kindly provided by Prof. Suk-Chul Bae (Chungbuk National University, Cheongju, South Korea). The myc-RUNX3 expression vector was transfected into HEK293 cells with Lipofectamine 2000 (Invitrogen). Transfected cells were treated with HDAC inhibitors at 1 μM the next day for an additional 24 h. Cells were lysed in ice-cold lysis buffer (25 mM HEPES, pH 7.5, 150 mM NaCl, 1% Nonidet P-40, 0.25% sodium deoxycholate, 10% glycerol, 25 mM NaF, 1 mM EDTA, 1 mM Na_3VO_4) and

cleared by centrifugation. For immunoprecipitation experiments, 500 mg of protein was incubated with anti-myc antibody and precipitated with protein G beads (Pierce) at 4°C. The beads were washed three times with cold lysis buffer, and the immunoprecipitates were analyzed by western blot with an antibody against acetylated lysine.

Reverse transcription polymerase chain reaction (RT-PCR). NCI-H460 cells were plated and treated with drugs the next day. After 24 h, cells were harvested. Total RNA was extracted with an RNeasy mini kit (Qiagen, Valencia, CA, USA) according to the manufacturer's protocol. First-strand cDNA synthesis was performed on 1 μg of total RNA with Superscript III reverse transcriptase according to the manufacturer's instructions (Invitrogen). The resulting first-strand cDNA was amplified to measure mRNA levels of RUNX3 with specific primers. Equal quantities of each sample were analyzed by 1.5% agarose gel electrophoresis and visualized with ethidium bromide staining and UV illumination. The mRNA level of glyceraldehyde phosphate dehydrogenase (GAPDH) served as an internal control for RT-PCR analysis. The following primers were used: 5′-GCA GGC AAT GAC GAG AAC TA-3′ (RUNX3 forward primer), 5′-GTC TGG TCC TCC AGC TTC TG-3′ (RUNX3 reverse primer), 5′-CAA AGT TCT CAT GGA TGA CC-3′ (GAPDH forward primer), 5′-CCA TGG AGA AGG CTG GGG-3′ (GAPDH reverse primer).

***In vivo* pharmacokinetic studies.** Animal studies were approved by the Institutional Animal Care and Use Committee at KRIBB and conducted as described previously[36] with minor modifications. Briefly, specific pathogen-free male Sprague–Dawley (SD) rats (10 weeks old, body weight 298–315 g), purchased from Koatech Co. (Kyeonggi, Republic of Korea), were given a single dose of **4l** intravenously (i.v.; 2 mg/kg, n = 3) or orally (p.o.; 10 mg/kg, n = 3).

Dosing solutions were prepared in dimethylacetamide (DMAC)/20% 2-hydroxypropyl-β-cyclodextrin (10/90, v/v%) for i.v. administration, and DMAC/Vitamin E TPGS 80/25% solutol HS 15 (10/10/80, v/v%) for p.o. administration, and administered at dosing volumes of 5 and 10 ml/kg for i.v. and p.o., respectively. A 100-μl aliquot of each plasma sample was prepared and three volumes of ice-cold acetonitrile containing carbamazepine (internal standard) were added. The mixture was centrifuged at 910 ×g for 10 min, and the supernatant was subjected to LC-MS/MS analysis. Pharmacokinetic parameters were calculated by standard noncompartmental analysis of plasma concentration–time profiles using Kinetica^{TM}4.4.1 (Thermo Fisher Scientific, Inc., Woburn, MA, USA). The areas under the plasma concentration–time curves (AUC) were calculated by the linear–trapezoidal method. Systemic plasma clearance (CL_p) was calculated as follows: CL_p = Dose/$AUC_{inf.}$ Terminal elimination half-life ($t_{1/2}$) was calculated by the following equation: $t_{1/2} = 0.693/\lambda_z$ where λ_z is the terminal disposition rate constant. Volume of distribution at steady state (V_{ss}) was calculated as follows: V_{ss} = Dose × $AUMC_{inf}/(AUC_{inf})^2$, where $AUMC_{inf}$ is the area under the first moment of the plasma concentration–time curve extrapolated to infinity. Oral bioavailability (F) was calculated as follows: F (%) = ($AUC_{p.o.}/AUC_{i.v.}$) × ($Dose_{i.v.}/Dose_{p.o.}$) × 100.

***In vivo* xenograft experiment.**

6-week-old female specified-pathogen-free (SPF) BALB/c nude mice were purchased from Charles River Laboratories (Yokohama, Japan) and maintained in accordance with the Animal Research Committee's Guidelines at the Korea Research Institute of Bioscience and Biotechnology (KRIBB). NCI-H460 cells (3×10^7/animal) were injected subcutaneously into the flank area. When tumors reached a volume of 50–80 mm^3, as measured with a digital caliper,

mice were randomized into groups of four animals each to receive either vehicle control or **4l**. The drugs were orally administered at 20 mg/kg in 10% DMAC and 10% Tween 80 (Sigma) in saline daily for two weeks. Tumor growth was measured three times a week until the end of the study. The length and width of the tumor were measured with calipers. Tumor volume was calculated according to the formula for an ellipse, volume = 0.523 × (long dimension) × (short dimension)^2.

Statistics software. The level of protein expression was quantified with Scion image densitometry software (Scion Corporation, Frederick, MD). Data were analyzed with a commercial statistics software package (SigmaStat, SPSS Science, Chicago, IL, USA). Student's *t*-test was performed for individual comparisons. Multiple comparisons were assessed by one-way ANOVA or regression analysis.

FIGURES

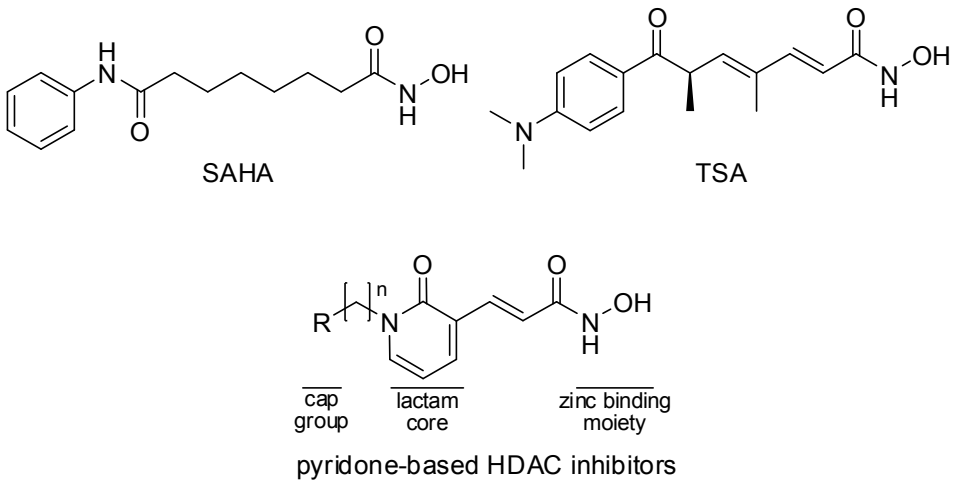

Figure 1. Chemical structures of hydroxamic acid-based HDAC inhibitors.

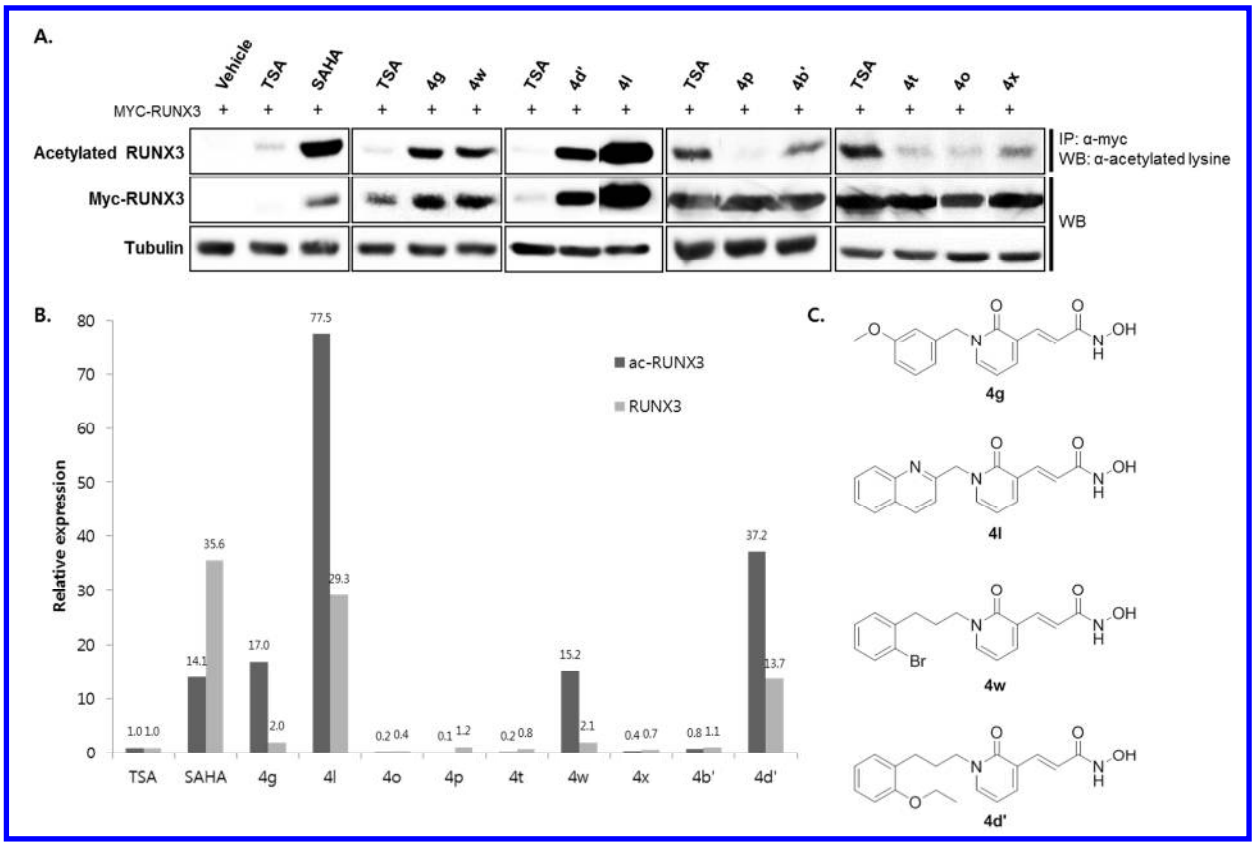

Figure 2. RUNX3 acetylation of selected pyridone-based HDAC inhibitors. A) Myc-tagged RUNX3 (Myc-RUNX3) was expressed in HEK293 cells. Acetylated RUNX3 levels were analyzed by immunoprecipitation in HEK293 cells following treatment with 1 μM of the indicated test compound; B) Relative expression of RUNX3 acetylation based on the results of

the western blot shown in Figure 2A (with 1 μM of the indicated test compound); C) Selected compounds based on the RUNX3 acetylation assay.

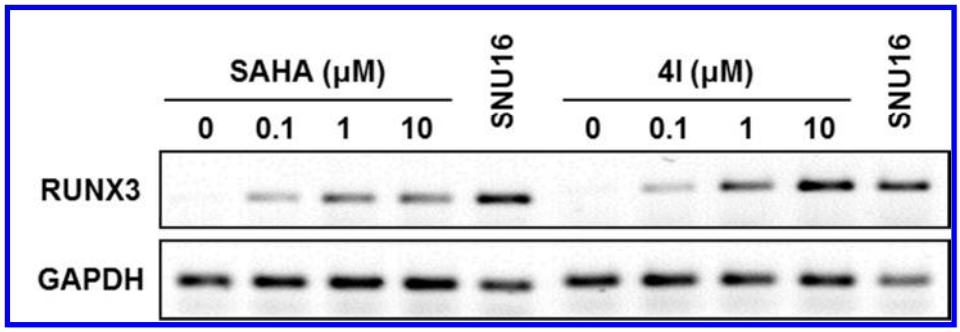

Figure 3. Dose-dependent effects of **4l** on RUNX3 mRNA expression in NCI-H460 cells. SNU16 gastric cancer cells were used as a positive control.

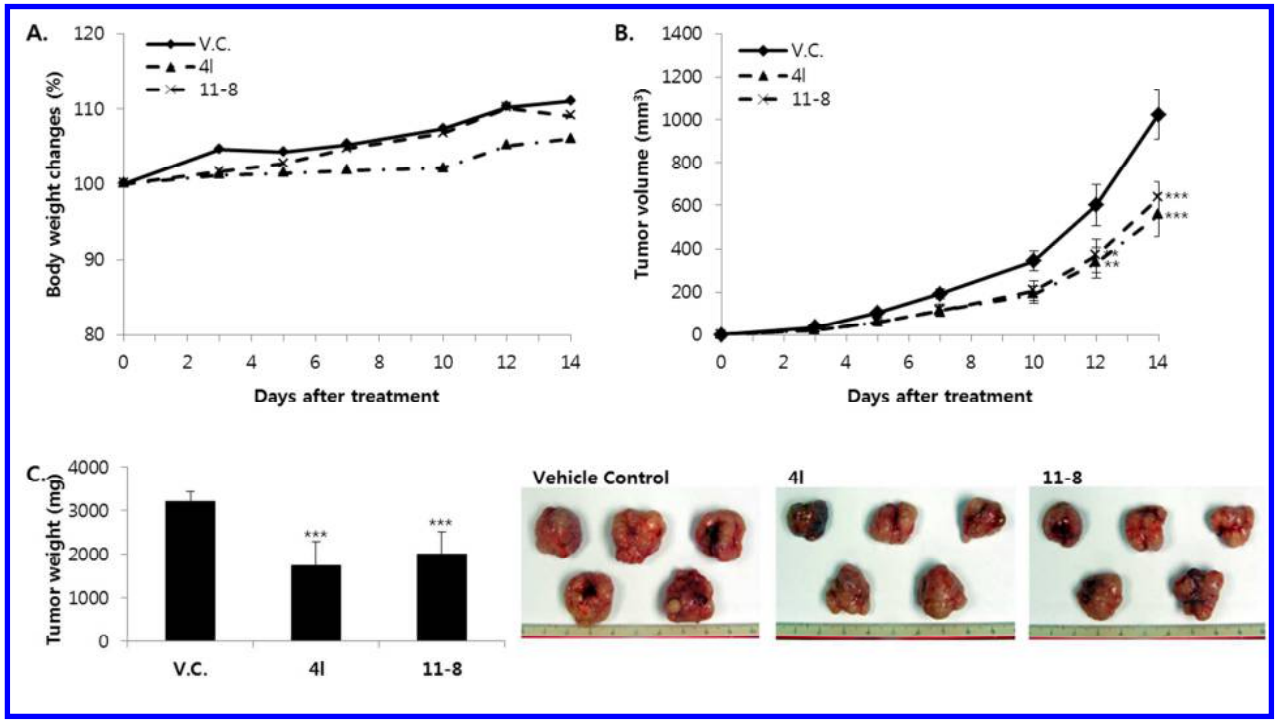

Figure 4. Effect of **4l**, 20 mg/kg, q1d × 14 on the growth of a NCI-H460 human lung tumor xenograft in nude mice: A) average body weight changes, B) average tumor volume, and C) average tumor weight in mice treated with vehicle control (V.C.), **11-8**, and **4l**. ***p*<0.01, ****p*<0.001, Student t-test. The standard deviations of each value are provided in table S6 and S7. ΔV_t (tumor volume) = V_t (measurement of the tumor volume) – V_0 (initial tumor volume).

SCHEMES

Scheme 1. General procedure for synthesis of pyridone-based HDAC inhibitors[a]

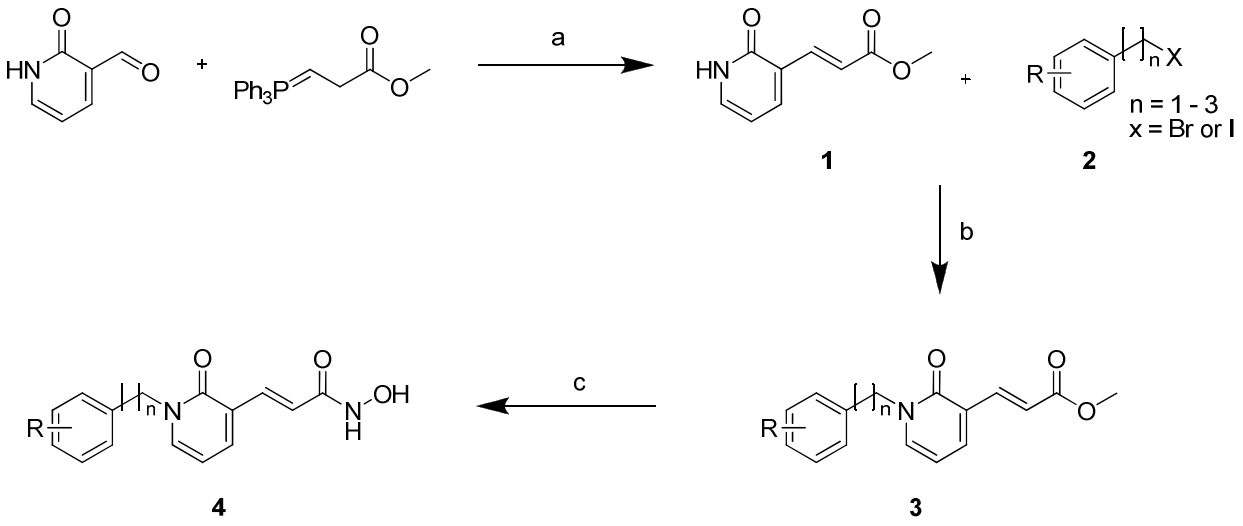

4a n = 1 R = 2-bromo
4b n = 1 R = 3-bromo
4c n = 1 R = 4-bromo
4d n = 1 R = 2-ethyl
4e n = 1 R = 4-ethyl
4f n = 1 R = 4-t-butyl
4g n = 1 R = 3-methoxy
4h n = 1 R = 4-methoxy
4i n = 1 R = 2-pyridinyl
4j n = 1 R = 3-pyridinyl
4k n = 1 R = 4-pyridinyl
4l n = 1 R = 2-quinolinyl
4m n = 2 R = 3-bromo
4n n = 2 R = 4-bromo
4o n = 2 R = 4-ethyl
4p n = 2 R = 4-t-butyl
4q n = 2 R = 3-methoxy
4r n = 2 R = 2-ethoxy
4s n = 2 R = 3-ethoxy
4t n = 2 R = 4-ethoxy
4u n = 2 R = 2-pyridinyl
4v n = 2 R = 4-pyridinyl
4w n = 3 R = 2-bromo
4x n = 3 R = 3-bromo
4y n = 3 R = 4-bromo
4z n = 3 R = 4-ethyl
4a` n = 3 R = 4-t-butyl
4b` n = 3 R = 3-methoxy
4c` n = 3 R = 4-methoxy
4d` n = 3 R = 2-ethoxy
4e` n = 3 R = 3-pyridinyl

[a]Reagents: (a) CH_2Cl_2, reflux; (b) K_2CO_3, acetone, reflux; (c) $KONH_2$ (1.7 M in MeOH), MeOH, 0°C

TABLES.

Table 1. Percentage of RUNX transcriptional activation relative to FGF-2, inhibition of HDAC enzyme activity, and cancer cell growth by pyridone-based analogues. The standard deviations of each value are provided in table S3–S5.

Compound	HDAC	RUNX	GI_{50} (μM)[a]					
	IC_{50} (μM)[a]	(%)[b]	PC-3	MDA-MB-231	ACHN	HCT-15	NCI-H23	NUGC-3
4a	0.19	86.0	2.88	1.59	1.53	2.40	2.30	1.66
4b	0.38	91.6	4.84	3.07	3.03	2.73	3.04	2.78
4c	0.10	99.2	1.88	2.49	1.48	4.31	3.00	2.11
4d	0.23	52.3	5.02	6.95	3.24	3.93	4.96	5.41
4e	0.10	74.3	2.07	3.68	1.54	1.86	2.35	1.67
4f	0.09	46.4	3.04	2.59	2.80	2.40	2.81	1.82
4g	0.15	200.0	1.82	3.18	1.26	2.60	2.69	1.69
4h	0.38	84.6	4.70	6.26	4.73	4.52	5.30	3.88
4i	0.46	35.6	10.22	>10	6.44	>10	>10	>10
4j	0.30	32.3	5.33	10.00	4.16	7.51	6.70	5.94
4k	0.42	69.1	9.17	4.92	9.49	>10	3.01	9.19
4l	0.03	687.5	0.49	0.10	0.25	0.38	0.13	0.71
4m	0.16	74.0	3.58	4.90	2.00	7.29	3.30	1.99
4n	0.36	53.5	4.84	6.39	2.14	8.60	3.04	2.83
4o	0.07	106.0	0.53	0.72	0.70	0.69	0.69	0.74
4p	0.11	104.7	0.50	0.84	0.70	0.71	0.91	0.47
4q	0.07	53.8	5.87	6.94	2.93	>10	5.06	2.91
4r	0.32	30.9	4.92	3.89	3.59	6.06	4.92	3.92
4s	0.12	76.9	1.34	1.74	0.94	0.92	1.81	1.42
4t	0.07	119.5	0.14	2.05	2.34	1.00	1.05	1.28
4u	3.94	26.7	>10	>10	>10	>10	>10	>10
4v	>10	19.6	>10	>10	>10	>10	>10	>10
4w	0.48	162.8	1.86	2.89	1.92	1.58	1.88	1.50
4x	0.10	100.8	1.26	1.85	0.74	1.16	1.22	1.20
4y	0.21	53.8	3.97	4.38	4.19	7.45	4.88	4.02
4z	0.31	14.3	1.85	2.88	1.71	1.06	2.15	1.74
4a'	0.38	34.4	1.48	2.23	1.83	1.42	1.78	1.31
4b'	0.03	142.1	0.70	0.72	0.76	1.59	0.87	1.05
4c'	0.14	97.6	1.78	1.36	0.98	0.90	1.31	0.97
4d'	0.05	105.5	0.18	0.56	0.32	0.66	0.46	0.47
4e'	0.57	30.0	>10	>10	>10	>10	5.21	>10
SAHA	0.11	80.2	2.69	2.00	4.22	2.49	2.34	2.94
Average								
1-carbon linker[c]	0.18	158.0	2.97	3.32	2.21	2.79	2.95	2.42
2-carbon linker[d]	0.16	77.4	2.71	3.43	1.92	3.61	2.60	1.95
3-carbon linker[e]	0.21	88.9	1.64	2.11	1.56	1.98	1.82	1.53

[a] Values are the means of a minimum of three independent experiments; [b] Values are the means of a minimum of two independent experiments; [c] Average activity of compounds **4a**-**4h** and **4l**; [d] Average activity of compounds **4m**-**4t**; [e] Average activity of compounds **4w**-**4d'**.

Table 2. Mouse liver microsomal stability of pyridone-based compounds

Compound	% Remaining, 30 mins[a]	
	NADPH(-)	NADPH(+)
4g	98.6 ± 0.0	61.5 ± 0.0
4l	100.0 ± 8.7	90.3 ± 4.4
4o	96.5 ± 0.0	11.1 ± 0.0
4p	103.1 ± 0.0	28.3 ± 0.0
4t	104.6 ± 0.0	59.6 ± 0.0
4w	93.3 ± 0.0	24.2 ± 0.0
4x	96.7 ± 0.0	20.7 ± 0.0
4b'	109.9 ± 4.0	88.4 ± 2.0
4d'	103.6 ± 1.3	31.5 ± 1.0
Buspirone[b]	100.8 ± 2.8	0.4 ± 0.0

[a] A 1-μM aliquot of the test compound was incubated with 0.5 mg/ml pooled mouse liver microsomes for 30 min at 37°C; [b] positive control.

Table 3. The rat and human liver microsomal stability of pyridone-based compounds

Compound	Species	% Remaining, 60 mins[a]			
		NADPH(-)	NADPH(+)	UDPGA(-)	UDPGA(+)
4l	Rat	92.0 ± 1.7	83.5 ± 1.7	88.9 ± 3.0	72.4 ± 2.3
	Human	74.7 ± 0.0	75.5 ± 2.2	95.2 ± 1.8	99.7 ± 4.5
4b'	Rat	116.0 ± 4.0	72.7 ± 5.2	81.3 ± 9.5	45.7 ± 5.7

[a] Microsomal stability was determined in liver microsomes (0.5 mg/ml) at 37°C using 1 μM test compounds (n = 2–3)

Table 4. Oral (PO) and intravenous (IV) pharmacokinetic (PK) parameters of **4l** in SD rats

PK parameter[a]		4l	
		IV	PO
Dose	(mg/kg)	2	10
$\mathbf{t_{max}}$	(hr)	NA	0.67 ± 0.14
$\mathbf{C_{max}}$	(ng/ml)	NA	142.1 ± 81.0
$\mathbf{AUC_{inf}}$[b]	(ng.hr/ml)	354.5 ± 5.6	863.3 ± 73.3
CL	(l/hr/kg)	5.6 ± 0.1	NA
$\mathbf{V_{ss}}$	(l/kg)	14.0 ± 2.2	NA
$\mathbf{t_{1/2}}$	(hr)	4.4 ± 0.8	10.3 ± 0.8
F	(%)	NA	**48.7 ± 4.1**

[a] PK parameters were based on mean plasma concentration-time profiles of three animals per time points. PK parameters were calculated by noncompartmental analysis using PK Solutions 2.0 (Summit Research Services, Montrose, CO, USA); [b] AUC after intravenous (-IV) administration was calculated from 0 to infinity, whereas the oral AUC was calculated from 0 to 5 h.

ASSOCIATED CONTENT

Supporting Information

Structural data of intermediates **3a-3e'**, final compounds **4a-4e'**, HPLC conditions and retention times of final compounds **4a-4e'**, *in silico* properties of **4a-4e'**, *in vitro* relative RUNX transcriptional activity in response to FGF-2, *in vitro* inhibitory activities against HDAC enzyme and human cancer cell lines of **4a-4e'**, and HDAC isoform selectivity of **4l**. This material is available free of charge via the Internet at http://pubs.acs.org.

AUTHOR INFORMATION

Corresponding Author

* Tel.: +82 2 2123 2882; fax: +82 2 362 7265; e-mail: gyoonhee@yonsei.ac.kr (G. Han)

* Tel.: +82 32 749 4509; fax: +82 32 749 4105; e-mail: organicjeong@yonsei.ac.kr (J. H. Jeong)

Author Contributions

The manuscript includes contributions from all authors. All authors have approved the final version of the manuscript.

ACKNOWLEDGMENT

We thank Prof. So Hee Kwon for helpful discussions. This research was supported by a grant from the Translational Research Center for Protein Function Control (NRF-2009-0083522), the Basic Science Research Program through the National Research Foundation of Korea (NRF) funded by the Ministry of Education (NRF-2013R1A1A2008165), Ministry of Health & Welfare (A120478), the Ministry of Science, ICT & Future Planning (NRF-2013M3A6A4072536), and the KRIBB Research Initiative Program.

ABBREVIATIONS

RUNX, runt related transcription factor; HDAC, histone deacetylase; HAT, histone acetyltransferase; TGF, transforming growth factor; TSA, trichostatin A; SAHA, suberoylanilide hydroxamic acid; PK, pharmacokinetics; EDC, N-(3-dimethylaminopropyl)-N’-ethylcarbodiimide hydrochloride; DMAP, 4-(dimethylamino)pyridine; PSA, polar surface area; UDPGA, uridine 5'-diphospho-glucuronic acid.

REFERENCES

(1) Arrowsmith, C. H.; Bountra, C.; Fish, P. V.; Lee, K.; Schapira, M. Epigenetic protein families: a new frontier for drug discovery. *Nat. Rev. Drug Discov.* **2012**, 11, 384-400.

(2) Fleming, C. L.; Ashton, T. D.; Gaur, V.; McGee, S. L.; Pfeffer, F. M. Improved synthesis and structural reassignment of MC1568: a class IIa selective HDAC inhibitor. *J. Med. Chem.* **2014**, 57, 1132-1135.

(3) McKinsey, T. A. Isoform-selective HDAC inhibitors: closing in on translational medicine for the heart. *J. Mol. Cell. Cardiol.* **2011**, 51, 491-496.

(4) Miller, T. A.; Witter, D. J.; Belvedere, S. Histone deacetylase inhibitors. *J. Med. Chem.* **2003**, 46, 5097-5116.

(5) Paris, M.; Porcelloni, M.; Binaschi, M.; Fattori, D. Histone deacetylase inhibitors: from bench to clinic. *J. Med. Chem.* **2008**, 51, 1505-1529.

(6) Lane, A. A.; Chabner, B. A. Histone deacetylase inhibitors in cancer therapy. *J. Clin. Oncol.* **2009**, 27, 5459-5468.

(7) Nakagawa, M.; Oda, Y.; Eguchi, T.; Aishima, S.; Yao, T.; Hosoi, F.; Basaki, Y.; Ono, M.; Kuwano, M.; Tanaka, M.; Tsuneyoshi, M. Expression profile of class I histone deacetylases in human cancer tissues. *Oncol. Rep.* **2007**, 18, 769-774.

(8) Yoo, C. B.; Jones, P. A. Epigenetic therapy of cancer: past, present and future. *Nat. Rev. Drug Discov.* **2006**, 5, 37-50.

(9) Vigushin, D. M.; Coombes, R. C. Targeted histone deacetylase inhibition for cancer therapy. *Curr. Cancer Drug Targets* **2004**, 4, 205-218.

(10) Popovic, R.; Licht, J. D. Emerging epigenetic targets and therapies in cancer medicine. *Cancer Discov.* **2012**, 2, 405-413.

(11) Wilting, R. H.; Dannenberg, J. H. Epigenetic mechanisms in tumorigenesis, tumor cell heterogeneity and drug resistance. *Drug Resist. Updat.* **2012**, 15, 21-38.

(12) Ivanov, M.; Kacevska, M.; Ingelman-Sundberg, M. Epigenomics and interindividual differences in drug response. *Clin. Pharmacol. Ther.* **2012**, 92, 727-736.

(13) New, M.; Olzscha, H.; La Thangue, N. B. HDAC inhibitor-based therapies: can we interpret the code? *Mol. Oncol.* **2012**, 6, 637-656.

(14) Rius, M.; Lyko, F. Epigenetic cancer therapy: rationales, targets and drugs. *Oncogene* **2012**, 31, 4257-4265.

(15) Singh, B. N.; Zhang, G.; Hwa, Y. L.; Li, J.; Dowdy, S. C.; Jiang, S. W. Nonhistone protein acetylation as cancer therapy targets. *Expert Rev. Anticancer Ther.* **2010**, 10, 935-954.

(16) Tang, J.; Yan, H.; Zhuang, S. Histone deacetylases as targets for treatment of multiple diseases. *Clin. Sci. (Lond)* **2013**, 124, 651-662.

(17) Chuang, L. S.; Ito, Y. RUNX3 is multifunctional in carcinogenesis of multiple solid tumors. *Oncogene* **2010**, 29, 2605-2615.

(18) Li, Q. L.; Ito, K.; Sakakura, C.; Fukamachi, H.; Inoue, K.; Chi, X. Z.; Lee, K. Y.; Nomura, S.; Lee, C. W.; Han, S. B.; Kim, H. M.; Kim, W. J.; Yamamoto, H.; Yamashita, N.; Yano, T.; Ikeda, T.; Itohara, S.; Inazawa, J.; Abe, T.; Hagiwara, A.; Yamagishi, H.; Ooe, A.; Kaneda, A.; Sugimura, T.; Ushijima, T.; Bae, S. C.; Ito, Y. Causal relationship between the loss of RUNX3 expression and gastric cancer. *Cell* **2002**, 109, 113-124.

(19) Tsang, Y. H.; Lamb, A.; Chen, L. F. New insights into the inactivation of gastric tumor suppressor RUNX3: the role of H. pylori infection. *J. Cell Biochem.* **2011**, 112, 381-386.

(20) Bae, S. C.; Lee, Y. H. Phosphorylation, acetylation and ubiquitination: the molecular basis of RUNX regulation. *Gene* **2006**, 366, 58-66.

(21) Li, Q. L.; Kim, H. R.; Kim, W. J.; Choi, J. K.; Lee, Y. H.; Kim, H. M.; Li, L. S.; Kim, H.; Chang, J.; Ito, Y.; Youl Lee, K.; Bae, S. C. Transcriptional silencing of the RUNX3 gene by

CpG hypermethylation is associated with lung cancer. *Biochem. Biophys. Res. Commun.* **2004**, 314, 223-228.

(22) Jin, Y. H.; Jeon, E. J.; Li, Q. L.; Lee, Y. H.; Choi, J. K.; Kim, W. J.; Lee, K. Y.; Bae, S. C. Transforming growth factor-beta stimulates p300-dependent RUNX3 acetylation, which inhibits ubiquitination-mediated degradation. *J. Biol. Chem.* **2004**, 279, 29409-29417.

(23) Lee, S. H.; Kim, J.; Kim, W. H.; Lee, Y. M. Hypoxic silencing of tumor suppressor RUNX3 by histone modification in gastric cancer cells. *Oncogene* **2009**, 28, 184-194.

(24) Wang, C.; Liu, Z.; Woo, C. W.; Li, Z.; Wang, L.; Wei, J. S.; Marquez, V. E.; Bates, S. E.; Jin, Q.; Khan, J.; Ge, K.; Thiele, C. J. EZH2 Mediates epigenetic silencing of neuroblastoma suppressor genes CASZ1, CLU, RUNX3, and NGFR. *Cancer Res.* **2012**, 72, 315-324.

(25) Cho, M.; Choi, E.; Kim, J. H.; Kim, H.; Kim, H. M.; Lee, J. I.; Hwang, K. C.; Kim, H. J.; Han, G. Lactam-based HDAC inhibitors for anticancer chemotherapy: restoration of RUNX3 by posttranslational modification and epigenetic control. *ChemMedChem* **2014**, 9, 649-656.

(26) Cho, M.; Choi, E.; Yang, J. S.; Lee, C.; Seo, J. J.; Kim, B. S.; Oh, S. J.; Kim, H. M.; Lee, K.; Park, S. K.; Kwon, H. J.; Han, G. Discovery of Pyridone-Based Histone Deacetylase Inhibitors: Approaches for Metabolic Stability. *ChemMedChem* **2013**, 8, 272-279.

(27) Choi, E.; Lee, C.; Cho, M.; Seo, J. J.; Yang, J. S.; Oh, S. J.; Lee, K.; Park, S. K.; Kim, H. M.; Kwon, H. J.; Han, G. Property-Based Optimization of Hydroxamate-Based gamma-Lactam HDAC Inhibitors to Improve Their Metabolic Stability and Pharmacokinetic Profiles. *J. Med. Chem.* **2012**, 55, 10766-10770.

(28) Kim, H. J.; Park, H. D.; Kim, J. H.; Cho, J. Y.; Choi, J. Y.; Kim, J. K.; Kim, H. J.; Shin, H. I.; Ryoo, H. M. Establishment and characterization of a stable cell line to evaluate cellular Runx2 activity. *J. Cell Biochem.* **2004**, 91, 1239-1247.

(29) Yoon, H. C.; Choi, E.; Park, J. E.; Cho, M.; Seo, J. J.; Oh, S. J.; Kang, J. S.; Kim, H. M.; Park, S. K.; Lee, K.; Han, G. Property based optimization of delta-lactam HDAC inhibitors for metabolic stability. *Bioorg. Med. Chem. Lett.* **2010**, 20, 6808-6811.

(30) Flipo, M.; Charton, J.; Hocine, A.; Dassonneville, S.; Deprez, B.; Deprez-Poulain, R. Hydroxamates: relationships between structure and plasma stability. *J. Med. Chem.* **2009**, 52, 6790-6802.

(31) Kim, H. M.; Oh, S. J.; Park, S. K.; Han, G.; Kim, K.; Lee, K. S.; Kang, J. S.; Nam, M.; Lee, K. In vitro metabolism of KBH-A40, a novel delta-lactam-based histone deacetylase (HDAC) inhibitor, in human liver microsomes and serum. *Xenobiotica* **2008**, 38, 281-293.

(32) Oh, S. J.; Lee, K.; Ryu, J.; Yu, H. E.; Han, G.; Park, S. K.; Kang, J. S.; Kim, H. M.; Kim, Y. C. Evaluation of the pharmacokinetics and metabolism of a novel histone deacetylase inhibitor, KBH-A40, in rats. *Xenobiotica* **2011**, 41, 155-163.

(33) Venkatesh, P. R.; Goh, E.; Zeng, P.; New, L. S.; Xin, L.; Pasha, M. K.; Sangthongpitag, K.; Yeo, P.; Kantharaj, E. In vitro phase I cytochrome P450 metabolism, permeability and pharmacokinetics of SB639, a novel histone deacetylase inhibitor in preclinical species. *Biol. Pharm. Bull.* **2007**, 30, 1021-1024.

(34) Dignam, J. D.; Lebovitz, R. M.; Roeder, R. G. Accurate transcription initiation by RNA polymerase II in a soluble extract from isolated mammalian nuclei. *Nucleic Acids Res.* **1983**, 11, 1475-1489.

(35) Skehan, P.; Storeng, R.; Scudiero, D.; Monks, A.; McMahon, J.; Vistica, D.; Warren, J. T.; Bokesch, H.; Kenney, S.; Boyd, M. R. New colorimetric cytotoxicity assay for anticancer-drug screening. *J. Natl. Cancer Inst.* **1990**, 82, 1107-1112.

(36) Lee, K.; Kwon, B. M.; Kim, K.; Ryu, J.; Oh, S. J.; Lee, K. S.; Kwon, M. G.; Park, S. K.; Kang, J. S.; Lee, C. W.; Kim, H. M. Plasma pharmacokinetics and metabolism of the antitumour drug candidate 2'-benzoyloxycinnamaldehyde in rats. *Xenobiotica* **2009**, 39, 255-265.

Table of Contents graphic